Collimator-detector response compensation in molecular SPECT reconstruction using STIR framework

Original Article

Hojjat Mahani[1,2], Gholamreza Raisali[1], Alireza Kamali-Asl[3] and Mohammad Reza Ay[2,4]

[1]Radiation Application Research School, Nuclear Science and Technology Research Institute, Tehran, Iran
[2]Research Center for Molecular and Cellular Imaging, Tehran University of Medical Science, Tehran, Iran
[3]Radiation Medicine Department, Shahid Beheshti University, Tehran, Iran
[4]Department of Medical Physics and Biomedical Engineering, Tehran University of Medical Science, Tehran, Iran

(Received 30 May 2016, Revised 28 August 2016, Accepted 1 September 2016)

ABSTRACT

Introduction: It is well-recognized that collimator-detector response (CDR) is the main image blurring factor in SPECT. In this research, we compensated the images for CDR in molecular SPECT by using STIR reconstruction framework.

Methods: To assess resolution recovery capability of the STIR, a phantom containing five point sources along with a micro Derenzo phantom were investigated. Influence of the lesion size on SPECT quantification was addressed by calculating recovery coefficients (RCs) as well as spill-over ratios (SORs) for reconstructed NEMA image-quality phantom. Impact of the resolution modeling on noise properties was also studied. The RCs were then compared with those of experimentally obtained. In all cases, the images were iteratively reconstructed using an OSEM algorithm with 4 subsets and 32 subiterations.

Results: CDR compensation gives rise to a significant drop in tomographic resolution from 2.45 mm to 1.55 mm. RC for hot rods of the NEMA IQ phantom monotonically grows as rod diameter increases, and results in an improvement of the RC up to a factor of 1.24 for the 5-mm rod diameter. PSF modeling also leads to a reduction in SOR from 0.24 to 0.16 averaged for the two cold cylinders. As a consequence of resolution recovery, a 15.5% overshoot near sharp edges imposing Gibbs ringing artifact occurs. In addition, a blobby noise texture is also observed. Furthermore, STIR results are consistent with the experimental ones.

Conclusion: Our findings demonstrate that resolution recovery is required for quantitative molecular SPECT imaging, and CDR compensation by the STIR framework offers superior SPECT image quality.

Key words: Image reconstruction; STIR; Molecular SPECT; Resolution recovery; Collimator-detector response

Iran J Nucl Med 2017;25(Suppl 1):26-34
Published: February, 2017
http://irjnm.tums.ac.ir

Corresponding author: Dr. Mohammad Reza Ay, Department of Medical Physics and Biomedical Engineering, Tehran University of Medical Sciences, Tehran, Iran. E-mail: mohammadreza_ay @sina.tums.ac.ir

INTRODUCTION

In molecular SPECT, spatial resolution is of great importance mainly because of animals' small-sized organs, and plays a crucial role in molecular imaging research [1-3]. In SPECT, the spatial resolution is primarily determined by collimator-detector response (CDR). The CDR results in a spatially varying and asymmetric reconstructed point spread function (PSF), leading to a blurred tomogram and consequently significantly affects accuracy and precision of radioactivity quantification [4].

Both analytic and iterative reconstruction approaches were implemented to compensate the CDR function, thus far. While analytic algorithms, utilizing a Metz filter, are usually fast and also easy-to-implement, but at the cost of neglecting distance dependency of spatial resolution. Thus, analytic approaches automatically result in an approximate compensation [5]. Iterative methods, whether maximum-likelihood expectation-maximization (MLEM) or other [6, 7], however can take both the CDR shape and the distance-dependent spatial resolution of the camera into consideration and provide CDR-compensated images superior to the analytic situations [8].

Tsui et al. [9], in 1988, proposed a method simultaneously implementing attenuation and detector response in SPECT. Three years after [10], they iteratively compensated SPECT images for CDR using multigrid method. Wang et al. [11], in 1999, compared analytic and iterative methods for the purpose of CDR compensation. In 2001, Bouwens and colleagues [12] tried to recover the lost resolution for list mode SPECT data. Liu et al. [13], in 2007, worked on CDR compensation in more details using an NCAT phantom and decomposing CDR into its components. Chun et al. [14] compensated SPECT images for CDR using point spread function (PSF) templates, in 2013. Zeraatkar and co-workers [15] developed a dedicated in-house image reconstruction algorithm, incorporating such a compensation for SPECT, in 2014.

Though, Software for Tomographic Image Reconstruction (STIR) is extensively used for PET reconstruction, but there are a limited number of studies performing the STIR for SPECT data, and to the extent of our knowledge, no study is benefitted from the STIR for CDR-compensated molecular SPECT reconstruction. Therefore, this work is first directed towards performing the STIR for analytic simulation of a high-resolution small-animal SPECT scanner, HiReSPECT [16-18], while CDR of the scanner is modeled during data acquisition period. Second, incorporating the CDR functions during iterative reconstruction, i.e., CDR compensation. Finally, quantifying the possible effects of CDR compensation on image quality through various phantom studies.

METHODS

STIR framework

STIR is an open source, object-oriented library implemented in C++ for emission tomography reconstruction. This library has been designed such that it can be used for many algorithms and scanner geometries [19]. Its third (current) version, STIR 3.0, allows for modeling 3D SPECT along with both attenuation and CDR corrections [20]. It should be noted that the STIR 3.0 is limited to modeling only parallel-hole collimated gamma cameras. In other words, other collimation systems (for example, pinhole collimators) cannot be currently modeled within the STIR.

The STIR presents a framework for both analytic (i.e., filtered-backprojection) as well as iterative (i.e., ordered-subset expectation-maximization (OSEM)) reconstruction algorithms with various data correction strategies. Furthermore, the STIR offers an environment for forward-projecting (or Radon transforming) the object being imaged and simultaneously degrading the data imposed by imaging physics. Thus, the STIR is capable of fully modeling an emission image formation. It should be noted that such a forward-projecting step is usually referred to analytic simulation in the literature.

Collimator-detector response

CDR of a SPECT system refers to the image generated from a point source of activity and the shape of the CDR is the primary factor determining the image resolution in SPECT [8]. The CDR is also referred to PSF in the literature, and is mainly a combination of four components: (1) geometric (collimator), (2) intrinsic detector, (3) septal scatter, and (4) septal penetration responses. The dominant is the geometric response. Compensating the SPECT images for the CDR mandates providing a prior knowledge of CDR functions at different distances from the collimator. Such prior data can be obtained by using either, analytic derivations, Monte Carlo simulations, or experimental measurements.

To experimentally obtain CDRs of the HiReSPECT scanner, a point source of ^{99m}Tc at various distances from the collimator's face was positioned [15]. The CDR of the scanner at other distances was linearly interpolated. In order to suppress additional noise propagation and artifacts during CDR-compensated image reconstruction, the CDRs are usually fitted to Gaussian functions, and consequently the fitted Gaussian shapes were considered as CDRs.

For parallel-hole collimated SPECT cameras, the spatial resolution is a linearly varying function of

source-to-collimator distance (SCD) and also is the same for all points having an identical SCD. Dependency of standard deviation of the CDR functions acquired by the HiReSPECT scanner on distance can be expressed as:

$$\sigma = 0.0155\, d + 1.17$$

where σ is the standard deviation of the Gaussian-modeled CDR and d is simply the SCD in mm. The standard deviation of a Gaussian function is its FWHM (usually referred as spatial resolution) divided by 2.355. The above mentioned equation was derived from the experiments [15].

Resolution recovery

To assess the STIR performance in recovery of the lost resolution, we designed and then reconstructed a phantom containing five point sources (12.5 mm spacing) to cover entire FOV of the head with and without resolution modeling. Data acquisition was completely implemented within STIR for 64 equally-angled projections using a ray-tracing method. During data acquisition, the CDRs were taken into consideration.

A digital micro-Derenzo phantom was modeled within the STIR to characterize the resolution enhancement as well. The phantom was simply a cylinder with a diameter of 32 mm and 35 mm length, and contains 6 sections of hot rods with diameters 1.6, 1.8, 2.0, 2.2, 2.4, and 2.6 mm. Having forward projected the phantom, the images were iteratively reconstructed using an OSEM algorithm with 4 subsets and 32 subiterations. The radius-of-rotation (ROR) was 25 mm.

Activity recovery

On the way to evaluate influence of object size in activity recovery, we then reconstructed NEMA NU-4 image-quality (IQ) phantom [21]. The NEMA IQ phantom is a cylinder of 30 mm in diameter and 50 mm in length, and contains three parts: (1) five rods with different diameters (1, 2, 3, 4, and 5 mm) and 20 mm in length, (2) a uniform part (15-cm in length), and (3) two cold (air-filled) cylinders. Activity recovery coefficient, or simply recovery coefficient (RC), was calculated for each rod as follows:

$$\mathrm{RC} = \frac{Maximum\ pixel\ value\ in\ the\ ROI\ sourronding\ each\ rod}{True\ activity\ (\frac{MBq}{cc})}$$

The ROIs were outlined so that they entirely surround each corresponding rod. Data acquisition condition and image reconstruction parameters were as for the pervious phantom studies. For a more realistic research, we added Poisson noise to the projection data prior to reconstruction using a STIR's built-in function.

Spreading out the background activity to the two air-filled cylinders (cold regions) was quantized as spill-over ratio (SOR), for a cylindrical volume of interest (VOI) using:

$$\mathrm{SOR} = \frac{Mean\ pixel\ value\ in\ each\ VOI}{Mean\ of\ the\ background}$$

The VOI was considered such that it surrounds central part of each cold phantom (6-mm in diameter and 10-mm in length). All SPECT data were reconstructed using the OSEM algorithm, with 4 subsets and 32 subiterations. Image grid was 128 × 128 × 64, resulting in voxel size of 0.3125 mm.

Noise characteristics

Influence of CDR compensation on noise texture was assessed by the uniform part of the NEMA image-quality phantom. The phantom was fully modeled within the STIR. The imaging protocol was 64 views over 360° and 25 mm ROR. In order to take statistical nature of the detected counts into account, the projection data were then subjected to a Poisson noise. The two datasets (noise-free and noise-present one) were iteratively reconstructed using the OSEM algorithm (4 subsets and 32 subiterations). Coefficient of variation (COV) in the reconstructed image was reported as noise level in the drawn ROI (a 22.5-mm diameter circular region over center of the image), using:

$$\mathrm{COV} = \frac{Standard\ deviation\ of\ pixel\ values\ in\ the\ ROI}{Mean\ pixel\ value\ in\ the\ ROI}$$

Alternatively, discrete noise power spectrum (NPS) of the noisy image was calculated as:

$$\mathrm{NPS}\ (k_x, k_y) = \frac{1}{MN}\left|\sum_{m=1}^{M}\sum_{n=1}^{N}(I(x,y) - \bar{I})\exp -2\pi i\,(xk_x + yk_y)\right|^2$$

where k_x and k_y are the spatial frequency corresponding to the x- and y-dimension, respectively. M and N are image dimentions, $I(x,y)$ is the noisy image, and $\bar{I}$ is the mean of the image $I(x,y)$.

Verification and validation

In the direction of verifying our OSEM reconstruction procedure, we reconstructed a 3D noiseless Shepp-Logan phantom using the STIR. Normalized mean square error (NMSE), as a metric indicating how well our STIR scheme is working, was then computed as follows:

$$\text{NMSE} = \frac{\sum_{i=1}^{N}\sum_{j=1}^{M}(I_{ij}-\hat{I}_{ij})^2}{\sum_{i=1}^{N}\sum_{j=1}^{M}I_{ij}^2}$$

where I_{ij} is the reconstructed image, $\hat{I}_{ij}$ is the original Shepp-Logan phantom, N and M are the image dimensions for a 2D slice.

In order to validate our STIR modeling, reconstruction and compensation, we compared the STIR-provided RCs with those of experimentally obtained by the HiReSPECT scanner benefitting from a dedicated resolution-recovery-embedded image reconstruction [16]. The experiments had conducted with data acquisition and condition as for our STIR study.

RESULTS

Resolution recovery

Figures 1a, 1b, and 1c reveal the STIR performance in recovery of the lost resolution for a phantom containing five equally-distance point sources. PSF correction using the STIR results in approximately uniform spatial resolution throughout the FOV. Figure 1d is line profile of the images across the yellow arrow comparing the original phantom and its corresponding PSFs without and with resolution recovery.

The digital micro-Derenzo phantom and its reconstructions without and with CDR compensation are depicted in Figures 2a, 2b, and 2c, respectively. Visual assessment proves that more details would be resolved in the phantom, when one utilizes CDR compensation.

Activity recovery

In Figures 3a, 3b, and 3c the hot rods part of the NEMA IQ phantom and the reconstructed phantom with and without PSF correction are depicted.

RC is then calculated for each rod of the phantom (totally 4 rods) with and without resolution recovery (Figure 3d), using related equation. Figures 4a, 4b, and 4c refer to the two cold cylinders embedded in a hot background (a part of NEMA IQ phantom), and its reconstruction without and with resolution modeling.

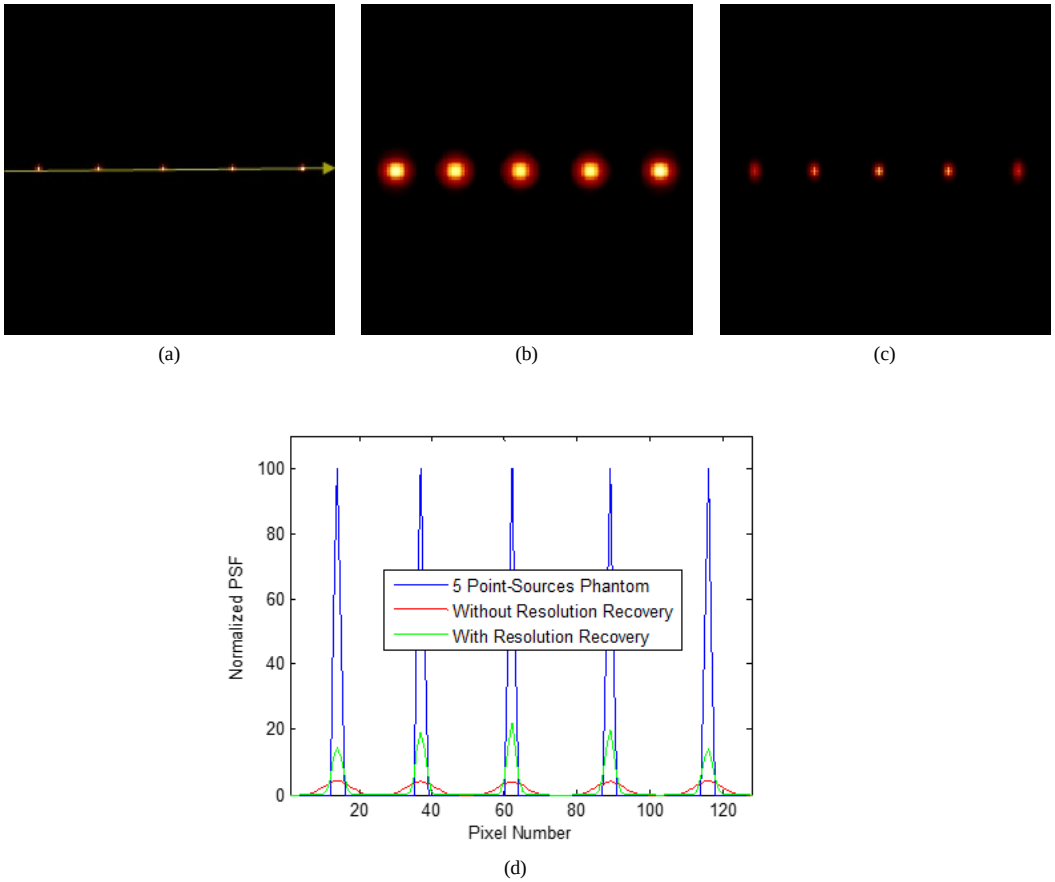

Fig 1. Five point-sources study: (a) the original phantom, (b) its reconstruction without CDR compensation, (c) with CDR compensation, and (d) a line-profile comparing uncorrected and CDR-corrected PSFs.

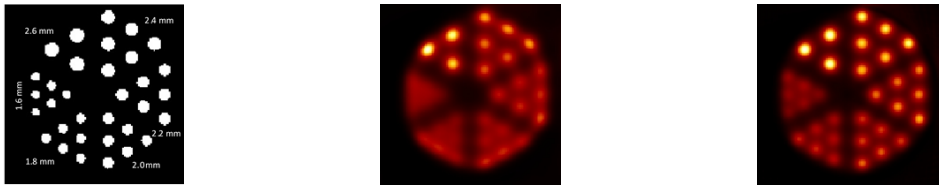

(a) (b) (c)

Fig 2. (a) Digital micro-Derenzo phantom, (b) no-PSF modeled reconstruction, and (c) PSF-corrected reconstruction. The images grid are 128×128 and pixel-size is 0.25 mm.

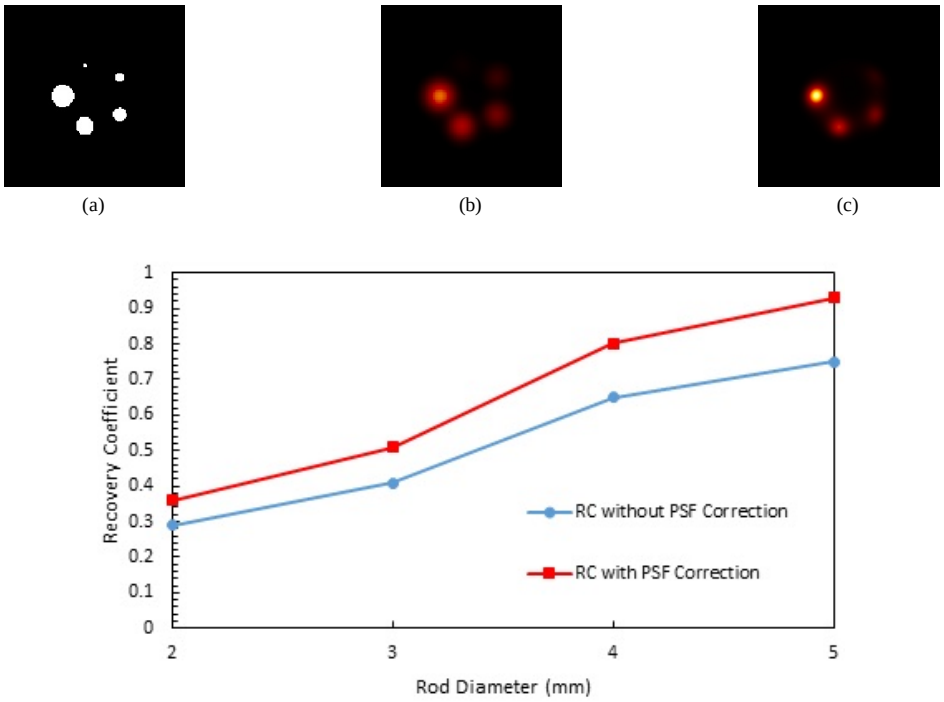

(a) (b) (c) (d)

Fig 3. (a) A slice of hot rods region of the NEMA IQ phantom, (b) no-PSF modeled reconstruction, (c) PSF-corrected reconstruction, and (d) RC as function of rod diameter. The images grid are 128 × 128 and pixel-size is 0.3125 mm.

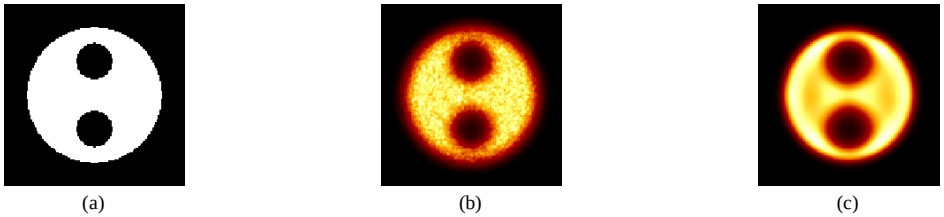

(a) (b) (c)

Fig 4. (a) A slice containing two cold cylinders in the NEMA IQ phantom, (b) no-PSF modeled reconstruction, (c) PSF-corrected reconstruction. The images grid are 128×128 and pixel-size is 0.3125 mm.

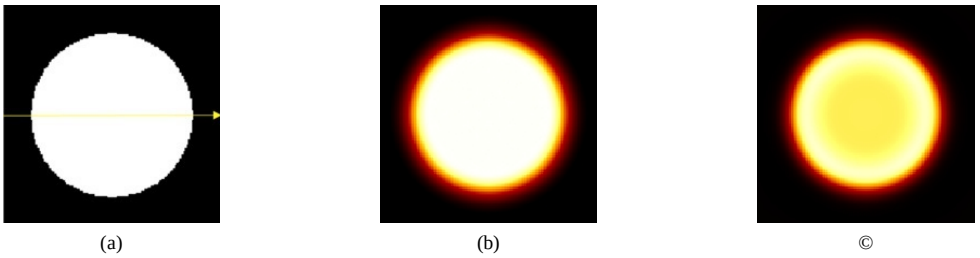

(a) (b) ©

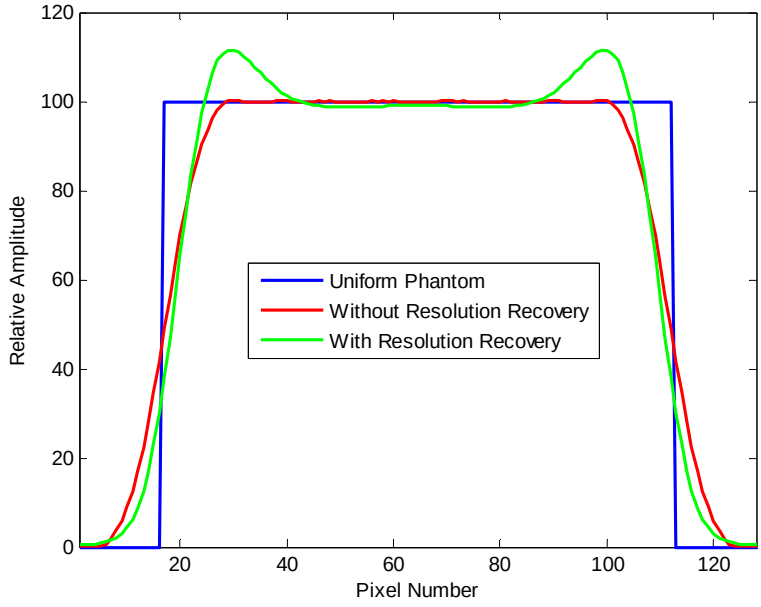

(d)

Fig 5. (a) A slice of uniform region of the NEMA IQ phantom, (b) no-PSF modeled reconstruction, (c) PSF-corrected reconstruction, and (d) line-profile of the images manifesting a ringing artifact in the case of PSF-corrected image. All datasets are noise-free.

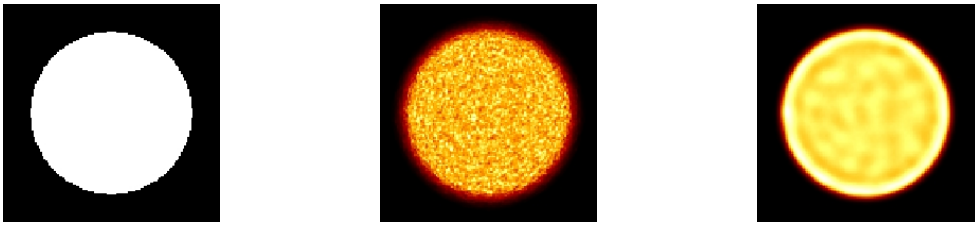

(a) (b) (c)

Fig 6. (a) A slice of uniform region of the NEMA IQ phantom, (b) no-PSF modeled reconstruction, and (c) PSF-corrected reconstruction. Projection data were corrupted by a Poisson noise.

Noise characteristics

Results from reconstruction of uniform part of the NEMA phantom with and without resolution recovery are shown in Figures 5a, 5b, and 5c, respectively. Figure 5d manifests Gibbs ringing artifact occurred at the edge of the phantom due to PSF correction process. Two overshoots are appeared at the sharp edges.

The effect of CDR compensation on image noise texture is visually highlighted in Figures 6a, 6b, and 6c. A Poisson noise is added to the projection data. As can be clearly observed, the resolution modeling significantly changes the noise texture. Figure 7 shows a normalized line profile of the 2D NPS of the noisy image, before and after PSF correction.

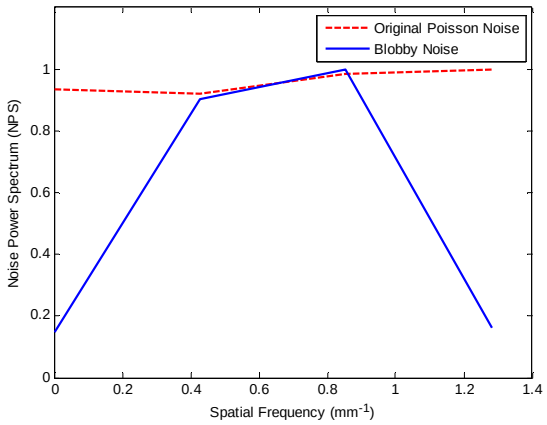

Fig 7. Noise power spectrum (NPS) is shown for the original Poisson noise and the blobby one (after PSF correction)

Verification and validation

A slice of the 3D Shepp-Logan phantom and its OSEM-reconstruction using the STIR are illustrated in Figure 8. NMSE, as described in the previous section, is 0.058.

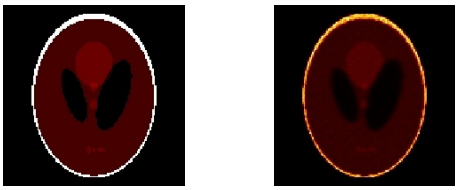

(a) (b)

Fig 8. (a) A slice of the 3D Shepp-Logan phantom and (b) its reconstruction using OSEM algorithm. The CDR is not incorporated during forward-projection step.

Figure 9, provides a comparison between our STIR reconstruction data and the experiments, for RCs. A good agreement (maximum 11% difference for the largest rod) between the STIR study and the experimental one is observed.

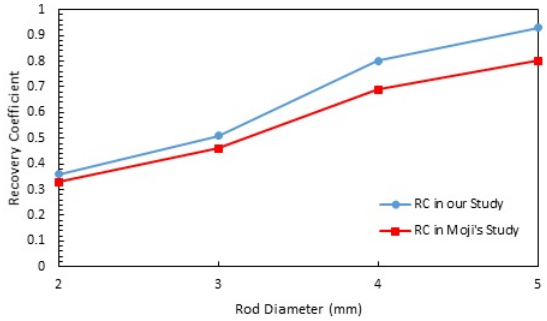

Fig 9. Comparison of the STIR-provided RCs with those of the Moji's study [16]. All RCs are after PSF-correction.

DISCUSSION

When we look at Figures 1a, 1b, and 1c, we can visually understand that the resolution recovery process inclines to uniformly recover the lost resolution across the FOV of the scanner. Therefore, one can conclude that the STIR performance in reconstruction along with resolution modeling of molecular SPECT data is promising. The more quantitative results are provided in Figure 1d, in which tomographic resolution improves from 2.45 mm to 1.55 mm after compensation of the image for CDR. Once upon resolution modeling, image contrast is significantly enhanced, as depicted in Figure 1d. In Figure 2, a substantial gain in spatial resolution is observed, and the rods with 1.6 mm diameter become resolvable when the image is compensated for the CDR (Figure 2c).

Because of the finite spatial resolution of the camera as well as discretizing the images into voxels, partial volume artifact occurs, especially for small-sized objects. Partial volume effect (PVE) results in spreading out the activity around the object, and leading to an underestimation in the case of hot lesions. PSF correction capability of the STIR makes the framework feasible to obtain a higher RC. As can be seen from Figure 3d, when the rod diameter increases, the RC monotonically increases, because the rod volume becomes larger in comparison to the imaging resolution. Referring to both Figures 1d and 3c, the STIR not only recovers the lost resolution, but also enhances image contrast and this is the main reason that the RCs increase. For the 2- and 5-mm diameter rods, the RC approximately reaches 0.39 and 0.93, respectively.

Averaged SOR for the two air-filled cold cylindrical regions of the NEMA IQ phantom was calculated 0.24 and 0.16 without and with CDR compensation in Figures 4b and 4c, respectively. Falling off the SOR is primarily because the PSF correction algorithm tries to avoid spreading out the activity into neighbor voxels. As such, similar to the hot lesions, PVE is mitigated via CDR compensation. Hence, the cold cylinders become more clear and larger.

In addition, the PSF correction process generates edge artifact (the Gibbs ringing artifact) [22]. The image oscillates and jumps at sharp edges resulting in an overshoot near such edges. Based upon Figure 5d, a 15.5% overshoot is observed at the edges of uniform part of the NEMA IQ reconstruction. Therefore, there is strict trade-off between image resolution and Gibbs artifact. However, various studies are comprehensively addressed such a compromise [23, 24].

Noise performance after PSF correction is a complex process in iterative reconstruction of the images, mostly due to nature of the CDR compensation algorithms [25]. A CDR compensation algorithm

tends to behavior as an apodized high-pass filter. Indeed, PSF correction recovers only those frequency components that are resolved by the scanner. For this reason, such a mechanism not only amplifies mid-frequency, but also simultaneously suppresses high-frequency components, and automatically gives rise to a correlated noise texture compared to the original approximate white (uncorrelated) noise. As a result, this can lead to a diminished image noise as Rahmim et al. predicted for PET imaging [22]. COV, as a spatial measure, of the reconstructed uniform part of the NEMA IQ phantom is 8.4% compared to the value of 6.7% after resolution recovery. Although, resolution modeling using the STIR yields a subtle decrease in image noise, but creates a blobby noise texture, as is manifested in Figure 6c. The NPS reflects frequency-dependence of the image noise. Figure 7 reflects that the NPS of a PSF-corrected image is no longer flat (as is resulted for the white noise) and is frequency band-limited. Therefore, the CDR correction algorithm alters the noise pattern to a correlated texture.

Referring to Figures 8a and 8b, a NMSE of 0.06 was found for reconstruction of 3D Shepp-Logan phantom using the STIR. Furthermore, there is a good agreement (maximum 11% difference for the 5-mm diameter cylinder) between the STIR-based PSF corrected RCs and those reported by the Moji's study [16] (Figure 9). The STIR benefits from an on-the-fly system matrix calculator algorithm for both image reconstruction and CDR compensation [19, 20], compared to the Zeraatkar's rotation-based projector/backprojector pair strategy [16]. While the rotation-based image reconstruction and CDR compensation algorithms are straightforward and fast but, they considerably suffer from interpolation errors. On the other hand, the difference between the STIR-provided results and preclinical data [16] also comes from other imaging physics phenomena, like photon attenuation as well as Compton scattering that are not included in our STIR research.

CONCLUSION

The purpose of this work has been to quantify compensation of molecular SPECT data for CDR of the scanner using STIR platform. According our findings, one can conclude that CDR compensation is mandatory, particularly in quantitative molecular SPECT, in order to obtain a high-quality and low-bias image by reducing PVE. Even though CDR compensation leads to a higher-resolution images but it is counterbalanced by a correlated noise pattern as well as notable edge artifact, and one should pay attention to such side-effects when compensating tomograms. There is an obvious advantage of the STIR for the purpose of quantitative SPECT reconstruction. Reconstruction capability of the STIR at the same time benefiting from both CDR and attenuation correction capabilities of this platform, makes the STIR a unique framework for quantitative molecular SPECT reconstruction.

Acknowledgments

This work was supported by Tehran University of Medical Science under grant No. 25938. The authors declare that they have no conflict of interest.

REFERENCES

1. Zaidi H. Molecular imaging of small animals: instrumentation and applications. 1st ed. New York: Springer;2014.
2. Kiessling F, Pichler BJ. Small animal imaging. 1st ed. New York: Springer;2011.
3. Meikle SR, Kench P, Kassiou M, Banati RB. Small animal SPECT and its place in the matrix of molecular imaging technologies. Phys Med Biol. 2005 Nov 21;50(22):R45-61.
4. Frey EC, Humm JL, Ljungberg M. Accuracy and precision of radioactivity quantification in nuclear medicine images. Semin Nucl Med. 2012 May;42(3):208-18.
5. Tsui BM, Frey EC, Zhao X, Lalush DS, Johnston RE, McCartney WH. The importance and implementation of accurate 3D compensation methods for quantitative SPECT. Phys Med Biol. 1994 Mar;39(3):509-30.
6. Shepp LA, Vardi Y. Maximum likelihood reconstruction for emission tomography. IEEE Trans Med Imaging. 1982;1(2):113-22.
7. Hudson HM, Larkin RS. Accelerated image reconstruction using ordered subsets of projection data. IEEE Trans Med Imaging. 1994;13(4):601-9.
8. Tsui BMW, Frey EC. Analytic image reconstruction methods in emission computed tomography. In: Zaidi H. Quantitative analysis in nuclear medicine imaging. Singapore: Springer;2006. p. 82-106.
9. Tsui BMW, Hu HB, Gilland DR, Gullberg GT. Implementation of simultaneous attenuation and detector response correction in SPECT. IEEE Trans Nucl Sci. 1988;35(1):778-83.
10. Tsui BMW, Zhao XD, Frey EC. Accurate 3D detector response compensation in SPECT using multigrid iterative reconstruction methods. IEEE Nucl Sci Symp Conf Rec. 1995;2:1151-1155.
11. Wang WT, Tsui BMW, Frey EC, Wessell DE. Comparison of an analytical and an iterative based collimator-detector response compensation method in SPECT. IEEE Nucl Sci Symp Conf Rec. 1998;2:1382-1386.
12. Bouwens LR, Gifford H, Van de Walle R, King MA, Lemahieu I, Dierckx RA. Resolution recovery for list-mode reconstruction in SPECT. Phys Med Biol. 2001 Aug;46(8):2239-53.
13. Liu S, Farncombe TH. Collimator-detector response compensation in quantitative SPECT reconstruction. IEEE Nucl Sci Symp Conf Rec. 2007;5:3955-3960.
14. Chun SY, Fessler JA, Dewaraja YK. Correction for collimator-detector response in SPECT using point spread function template. IEEE Trans Med Imaging. 2013 Feb;32(2):295-305.

15. Zeraatkar N, Sajedi S, Farahani MH, Arabi H, Sarkar S, Ghafarian P, Rahmim A, Ay MR. Resolution-recovery-embedded image reconstruction for a high-resolution animal SPECT system. Phys Med. 2014 Nov;30(7):774-81.

16. Moji V, Zeratkar N, Farahani MH, Aghamiri MR, Sajedi S, Teimourian B, Ghafarian P, Sarkar S, Ay MR. Performance evaluation of a newly developed high-resolution, dual-head animal SPECT system based on the NEMA NU1-2007 standard. J Appl Clin Med Phys. 2014 Nov 8;15(6):4936.

17. Sajedi S, Zeraatkar N, Moji V, Farahani MH, Sarkar S, Arabi H, Teymooriana B, Ghafarian P, Rahmim A, Ay MR. Design and development of a high resolution animal SPECT scanner dedicated for rat and mouse imaging. Nucl Instr Meth Phys Res A. 2014;741:169-76.

18. Pashazadeh AM, Tanha K, Jafarian-Dehkordi F, Assadi M, Moji V, Zeraatkar N, Ay MR. Experimental evaluation of the performance of HiReSPECT scanner: a high-resolution SPECT system for small-animal imaging. Front Biomed Technol. 2014;1(3):222-227.

19. Thielemans K, Tsoumpas C, Mustafovic S, Beisel T, Aguiar P, Dikaios N, Jacobson MW. STIR: software for tomographic image reconstruction release 2. Phys Med Biol. 2012 Feb 21;57(4):867-83.

20. Fuster BM, Falcon C, Tsoumpas C, Livieratos L, Aguiar P, Cot A, Ros D, Thielemans K. Integration of advanced 3D SPECT modeling into the open-source STIR framework. Med Phys. 2013 Sep;40(9):092502.

21. NEMA Standards Publication NU 4-2008. Performance measurements of small animal positron emission tomographs (PETs). National Electrical Manufacturers Association; 2008.

22. Rahmim A, Qi J, Sossi V. Resolution modeling in PET imaging: theory, practice, benefits, and pitfalls. Med Phys. 2013 Jun;40(6):064301.

23. Tong S, Alessio AM, and Thielemans K, Stearns C, Ross S, Kinahan PE. Properties and mitigation of edge artifacts in PSF-based PET reconstruction. IEEE Trans Nucl Sci. 2011;58(5) 2264-2275.

24. Zeng GL. Gibbs artifact reduction by nonnegativity constraint. J Nucl Med Technol. 2011 Sep;39(3):213-9.

25. Nuyts J. Unconstrained image reconstruction with resolution modeling does not have a unique solution. Eur J Nucl Med Mol Imaging Phys. 2014;1:98.